Journal of Food Engineering 118 (2013) 406–416

Contents lists available at SciVerse ScienceDirect

Journal of Food Engineering

journal homepage: www.elsevier.com/locate/jfoodeng

Development of a computer simulation model for processing food in a microwave assisted thermal sterilization (MATS) system

F.P. Resurreccion Jr. [a,d], J. Tang [a,*], P. Pedrow [b], R. Cavalieri [c], F. Liu [a], Z. Tang [a]

[a] Biological Systems Engineering Department, Washington State University, Pullman, WA 99164, USA
[b] School of Electrical Engineering and Computer Science, Washington State University, Pullman, WA 99164, USA
[c] Agricultural Research Center, College of Agricultural, Human, and Natural Resource Sciences, Washington State University, Pullman, WA 99164, USA
[d] Corporate R&D, Graphic Packaging International, Golden, CO 80403, USA

ARTICLE INFO

Article history:
Received 28 November 2012
Received in revised form 18 February 2013
Accepted 22 April 2013
Available online 2 May 2013

Keywords:
Microwave heating
Computer simulation
Chemical marker

ABSTRACT

The microwave assisted thermal sterilization computer simulation model (MATS-CSM) was developed to improve the previous computer simulation model for the microwave assisted thermal sterilization (MATS) system. Development of the new MATS-CSM included determination of optimum heating time step, evaluation of electromagnetic field distribution and the resulting heating pattern in food, and experimental validation of heating patterns. It was determined that the minimum number of discretization that would not cause immediate divergence of the EM-heat transfer solution was 32 steps corresponding to 97 mm and 5.6 s of displacement and heating time for every step, respectively. Furthermore, this study successfully demonstrated the symmetrical electromagnetic field distribution between top and bottom microwave entry ports and a staggered electric field pattern from one cavity of the MATS to the next. In addition, MATS-CSM confirmed that incorporating heat diffusion in the simulation model reduces the difference in hot spot and cold spot temperature by 65%. It also confirmed that water circulation reduces the edge heating effect, as observed in experiments. The heating pattern generated by MATS-CSM was verified experimentally through a chemical marker method. Based on the percent areal cross section of the weighted average temperature, there were no noticeable differences between the heating zones generated by the MATS-CSM and by the chemical marker method. The percent areal cross section of the cold area 1, cold area 2, and hot area by MATS-CSM were 35%, 25%, and 40%, respectively, and the cold area 1, cold area 2, and hot area by chemical marker method were 35%, 30%, and 35%, respectively.

1. Introduction

A significant attribute of processing food in a microwave assisted thermal sterilization (MATS) system is the improved quality of the food due to the reduction of the processing time by as much as 10 times when compared to conventional heating methods (Brody, 2011; Guan et al., 2002; Tang et al., 2002, 2008). Although the advantages of using microwave energy are obvious, several challenges must be overcome to fully utilize microwave energy in thermal sterilization of food. One of which is the problem of uniformity in the electromagnetic (EM) field distribution (Metaxas and Meredith, 1993). The fundamental physics of the system pertaining to the design and operating frequency of the microwave cavity as well as the shape, size, placement, and dielectric properties of food can influence uniformity of EM field distribution (Kashyap and Wyslouzil, 1977; Ryynanen and Ohlsson, 1996; Romano et al., 2005; Geedipalli et al., 2007). Another notable challenge in using microwave energy is the edge overheating effect in food, which is a non-resonant phenomenon caused by the electric field parallel to the edge of the food (Risman, 2009).

Challenges in using microwave energy were overcome in the MATS system by designing and fabricating microwave cavities that operate in a single-mode with or without load (i.e., food) (Tang et al., 2006; Pathak et al., 2003). This was possible by using a 915 MHz microwave source of longer wavelength, instead of the more popular 2450 MHz, allowing for flexibility in the design of cavities with practical geometry and configuration (Brody, 2011). Since a single-mode cavity has only one resonant mode (Metaxas and Meredith, 1993; Decareau, 1985), the EM field pattern inside is always consistent and predictable.

In the MATS system, to lessen the effect of edge overheating, water is circulated inside the cavities together with the food being processed. The circulating water has three purposes: (1) it acts as a heat sink to reduce the edge overheating in food during microwave processes, (2) it maintains the temperature of the food once it reaches sterilization temperature (Tang et al., 2006), and (3) it acts as a matching medium resulting in a relatively even power deposition profile over the surface of the food (Pathak et al., 2003).

* Corresponding author.
E-mail address: jtang@wsu.edu (J. Tang).

0260-8774/$ - see front matter © 2013 Elsevier Ltd. All rights reserved.
http://dx.doi.org/10.1016/j.jfoodeng.2013.04.021

Computer simulation is a widely accepted tool that aids engineers in designing microwave ovens (Sundberg et al., 1996; Celuch and Kopyt, 2009; Hossan et al., 2010; Celuch et al., 2011). In developing the MATS system, computer simulation provided a theoretical basis for the design of the geometry of the cavities. Pathak et al. (2003) used a finite-difference time-domain (FDTD) numerical method to characterize the microwave field distribution inside the microwave cavities of MATS. It was demonstrated that the circulating water in the cavities helps to level the power distribution within the food. Following the work of Pathak et al. (2003), Chen et al. (2008) developed a computer simulation model using a similar FDTD numerical method that included both microwave propagation and heat transfer to simulate the continuous operation of the MATS system with the purpose of describing the heating pattern and location of the cold spot in food packages. Furthermore, Chen et al. (2008) developed a method of controlling the electromagnetic field distribution by way of placing an Ultem™ slab of specific thickness on the narrow wall of the cavities of MATS. The computer simulation model by Chen et al. (2008) was created only for a specific configuration and provides no provision for modification of the geometry of the cavities and the shape of food packages. Furthermore, considering that MATS is in its commercialization phase, scale-up will undoubtedly require several changes to the original configuration necessitating adjustments in the computer simulation. Thus there is a need to revise the tool.

1.1. Microwave assisted thermal sterilization (MATS) system

The pilot scale MATS (Fig. 1) at Washington State University is a closed system consisting of four sections—preheating, microwave heating, holding and cooling—arranged in series representing the four sequential processing steps. Each section has a separate water circulation system that consists of a pressurized tank and plate heat exchanger to control water flow at a pre-set temperature. A pocketed mesh conveyor belt made of non-metallic material extending from one end of the preheating section to the other end of the cooling section conveys food trays or pouches across different sections of MATS. This study is primarily concerned with the microwave heating section of the MATS. The MW heating section consists of four connected rectangular microwave cavities (i.e., cavity 1, cavity 2, cavity 3, and cavity 4) (Fig. 1). Each of the four cavities is connected to a separate corresponding microwave generator (generator 1, generator 2, generator 3, and generator 4), with stub tunners to minimize reflected power.

1.2. Features of MATS-CSM

In this study, the new computer simulation model is referred to as the MATS-CSM (microwave assisted thermal sterilization computer simulation model). The MATS-CSM employs a similar numerical approach as described by Chen et al. (2008) but also addresses the limitations of the previous version. Listed below are the critical limitations of Chen et al.'s (2008) computer simulation model that were the focus of the revisions done in the MATS-CSM:

- In the simulation model of Chen et al. (2008), the food packages were monitored as if they were equally spaced as they traveled through the four heating cavities with only six discrete steps per cavity (total of 24 steps for the four cavities) representing a pseudo-moving package. This scheme limits the number of discrete steps since it would not allow food packages to simultaneously and adjacently occupy an analytical zone. In this study, the MATS-CSM simulates moving food by replacing the media parameter of the volume that will be occupied on the next discrete step with the media parameter of the food, thereby eliminating the limit to the number of discrete steps.
- Chen et al. (2008) describe a two-cavity system on a one-cavity simulation model for an earlier version of MATS by executing the simulation twice (i.e., first simulation for the first cavity and second simulation for the second cavity). The grid for the finite difference calculation was terminated using a perfect electric conductor (PEC) resulting in almost a 2% error in EM field calculation per simulation (Chen et al., 2007). In this study, the MATS-CSM includes four cavities in one model eliminating the need for multiple executions of simulation. Furthermore, the right end of the first cavity and the left end of the fourth cavity of the MATS-CSM are extended such that the PEC termination is far from the bulk of the computational domain. Doing so reduces the error due to the PEC termination down to <0.5%.
- The simulation in Chen et al. (2008) requires node transformation to synchronize electromagnetic node with the temperature node for heat transfer. Using the new version of QuickWave™ v7.5 to create the MATS-CSM, thermal-FDTD uses the same mesh as with EM-FDTD (Celuch et al., 2011), thereby eliminating the need for node transformation and avoiding numerical diffusion error (Kopyt and Celuch, 2003, 2004).
- The heat transfer equation in Chen et al.'s (2008) simulation model is very specific to the node defined in the model. If there is a change in meshing, modification in the geometry of the cavity, or change in size, shape and composition of food package geometry, the heat transfer equation of Chen et al. (2008) will no longer work. In the MATS-CSM, for flexibility, all components are defined in an individual object with variable parameters that can be changed depending on the objectives of the user, and the mesh automatically readjusts to accommodate changes in the parameters.

1.3. MATS-CSM assumptions

1. The electromagnetic simulation region includes only cavities (not waveguides and only the exit apertures of the horn antennas which become ports in our simula-

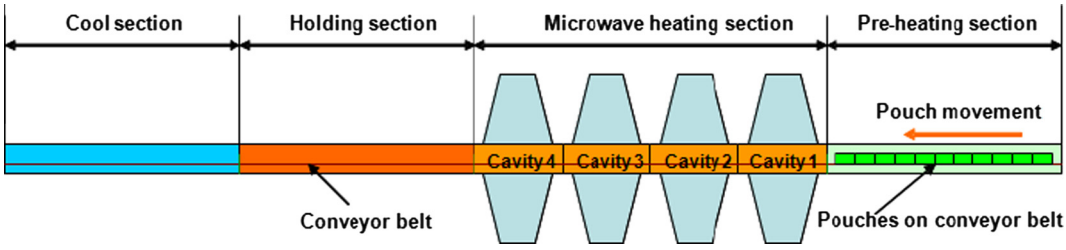

Fig. 1. Microwave assisted thermal sterilization (MATS) system diagram showing various sections: preheating, microwave heating, holding, and cooling.

tion). By way of the uniqueness theorem (Balanis, 1989), only the *E*-field in the plane of the input ports must be specified. Thus, incident and reflected fields in the horn antenna volume are not needed.
2. Since reflection occurs in the actual MATS system, the total microwave energy injected into each cavity in MATS-CSM is only the net transmitted microwave energy measured in the MATS system.
3. The transmitted microwave energy in the side arm of the *E*-plane tee-junction is evenly divided into its coplanar arms (i.e., Power/2) whose amplitude is equal to $\sqrt{2P}$. This assumption follows an ideal lossless reciprocal *E*-plane tee-junction (Pozar, 2005).
4. Waveguide parts such as elbows, tee-junction, spaces, circulator, probe-tuner, and directional coupler do not alter the characteristics of the electromagnetic wave (Chen et al., 2008).
5. Non-solid components of food sample (Alfredo sauce), due to its high viscosity and relatively small quantity, is assumed to have insignificant mobility. Therefore, heat transfer occurring within the Alfredo sauce and the Alfredo sauce – whey protein gel (WPG) boundary is assumed to be purely conductive.
6. Each element (characterized by a certain medium) occupying a certain volume is assumed to be linear, homogeneous, isotropic, and non-dispersive.
7. The turbulent condition of circulating water in the cavities is considered in MATS-CSM by defining the convective heat transfer coefficient between the boundary of circulating water and food.

1.4. Objective

The general objective of this study is to create a new computer simulation model for the microwave assisted thermal sterilization (MATS) system (which will be known as the MATS-CSM) that considers the coupled solution of electromagnetic field and heat transfer phenomena in food packages moving in multiple microwave cavities. The specific objectives of this study are:

- To create a flexible computer simulation model that is able to accommodate future modification in the MATS system. The MATS-CSM should be able to consider a wide range of food materials and package geometries, including both homogeneous and heterogeneous types of food.
- To describe electromagnetic field distribution inside microwave cavities with and without food packages.
- To determine the acceptable discrete number of time steps for the movement of food.
- To compare heating patterns in certain food packages considering EM-only solution versus EM-heat transfer solution.
- To validate the heating pattern output of the MATS-CSM through the chemical marker method.

2. Experimental procedure

2.1. Finite-difference time-domain (FDTD) governing equations

The set of four Maxwell equations that govern the general characteristics of electromagnetic waves traveling in a certain medium are:

$$\nabla \cdot \vec{D} = \rho \tag{1}$$

$$\nabla \cdot \vec{B} = 0 \tag{2}$$

$$\nabla \times \vec{E} = -\mu \frac{\partial \vec{H}}{\partial t} \tag{3}$$

$$\nabla \times \vec{H} = \sigma \vec{E} + \varepsilon \frac{\partial \vec{E}}{\partial t} \tag{4}$$

where $\vec{D}$, $\vec{B}$, $\vec{E}$, and $\vec{H}$ are the electric flux density, magnetic flux density, electric field intensity, and magnetic field intensity, respectively. The σ, μ, and ε are the electric conductivity, permeability, and permittivity of the material, respectively (Guru and Hiziroglu, 2004). In 3-dimensional (3D) space Eqs. (3) and (4) can be written as:

$$\nabla \times \vec{E} = \begin{vmatrix} \hat{a}_x & \hat{a}_y & \hat{a}_z \\ \frac{\partial}{\partial x} & \frac{\partial}{\partial y} & \frac{\partial}{\partial z} \\ E_x & E_y & E_z \end{vmatrix} = -\mu \frac{\partial \vec{H}}{\partial t} \tag{5}$$

$$\nabla \times \vec{H} = \begin{vmatrix} \hat{a}_x & \hat{a}_y & \hat{a}_z \\ \frac{\partial}{\partial x} & \frac{\partial}{\partial y} & \frac{\partial}{\partial z} \\ H_x & H_y & H_z \end{vmatrix} = \sigma \vec{E} + \varepsilon \frac{\partial \vec{E}}{\partial t} \tag{6}$$

For irregular or complex geometry, there is no closed-form solution to Eqs. (5) and (6) therefore; the most appropriate approach is to solve the equation numerically. The numerical approach works by discretizing the irregular or complex geometry (known as the computational volume) into cells or regular geometries. Finite-difference time-domain (FDTD) is a common numerical method for electromagnetic problems designed specifically to solve the time differentiated Maxwell's curl equations (Eqs. (5) and (6)). The FDTD method is a time-marching procedure that simulates the continuous electromagnetic waves in a finite spatial region while time-stepping continues until a desired simulation time is achieved or a stable field pattern is established (Taflove and Hagness, 2005). The unit cell in FDTD has a size equal to Δx, Δy, and Δz in the x, y, and z direction, respectively, at a given time step Δt. Considering the coordinate of a unit cell as grid point (m, n, p), the x, y, and z distance of any grid point would be $x = m\Delta x$, $y = n\Delta y$, and $z = p\Delta z$. Discretization of time follows in the same manner wherein a certain point in time q at the grid corresponds to a certain time by considering a time step Δt (i.e., $t = q\Delta t$).

In FDTD, the linear equation representation of the partial differential equation with respect to time is given by:

$$\frac{\partial H_i}{\partial t} = \frac{H_i^{q+1/2}(m,n,p) - H_i^{q-1/2}(m,n,p)}{\Delta t}$$

$$\frac{\partial E_i}{\partial t} = \frac{E_i^{q+1}(m,n,p) - H_i^{q}(m,n,p)}{\Delta t} \tag{7}$$

and the linear equation representation of the partial differential equation with respect to position considering central difference is given by:

$$\frac{\partial F_i}{\partial x} = \frac{F_i^{q}(m+1,n,p) - F_i^{q}(m,n,p)}{\Delta x}$$

$$\frac{\partial F_i}{\partial y} = \frac{F_i^{q}(m,n+1,p) - F_i^{q}(m,n,p)}{\Delta y}$$

$$\frac{\partial F_i}{\partial z} = \frac{F_i^{q}(m,n,p+1) - F_i^{q}(m,n,p)}{\Delta z} \tag{8}$$

where F is either electric, E, or magnetic H field component.

The electric field is dependent on the updated magnetic field ($H_i^{q+1/2}$) and for the next time step on the grid, the magnetic field would be dependent on the updated electric field (E_i^{q+1}). The

routine of updating fields mimics a time-marching procedure of a simulating electromagnetic fields as described by Taflove (2005). The equations of the update of the field on the next time step are the following (Taflove and Hagness, 2005):

$$H_x^{q+\frac{1}{2}}\left(m,n+\frac{1}{2},p+\frac{1}{2}\right)=H_x^{q-\frac{1}{2}}\left(m,n+\frac{1}{2},p+\frac{1}{2}\right)+\left\{\frac{\Delta t}{\mu\Delta z}\left[E_y^q\left(m,n+\frac{1}{2},p+1\right)-E_y^q\left(m,n+\frac{1}{2},p\right)\right]-\frac{\Delta t}{\mu\Delta y}\left[E_z^q(m,n+1,p+\frac{1}{2})-E_z^q\left(m,n,p+\frac{1}{2}\right)\right]\right\} \quad (9)$$

$$H_y^{q+\frac{1}{2}}\left(m+\frac{1}{2},n,p+\frac{1}{2}\right)=H_y^{q-\frac{1}{2}}\left(m+\frac{1}{2},n,p+\frac{1}{2}\right)+\left\{\frac{\Delta t}{\mu\Delta x}\left[E_z^q\left(m+1,n,p+\frac{1}{2}\right)-E_z^q\left(m,n,p+\frac{1}{2}\right)\right]-\frac{\Delta t}{\mu\Delta z}\left[E_x^q\left(m+\frac{1}{2},n,p+1\right)-E_x^q\left(m+\frac{1}{2},n,p\right)\right]\right\} \quad (10)$$

$$H_z^{q+\frac{1}{2}}\left(m+\frac{1}{2},n+\frac{1}{2},p\right)=H_z^{q-\frac{1}{2}}\left(m+\frac{1}{2},n+\frac{1}{2},p\right)+\left\{\frac{\Delta t}{\mu\Delta y}\left[E_x^q\left(m+\frac{1}{2},n+1,p\right)-E_x^q\left(m+\frac{1}{2},n,p\right)\right]-\frac{\Delta t}{\mu\Delta x}\left[E_y^q\left(m+1,n+\frac{1}{2},p\right)-E_y^q\left(m,n+\frac{1}{2},p\right)\right]\right\} \quad (11)$$

$$E_x^{q+1}\left(m+\frac{1}{2},n,p\right)=\frac{1-\frac{\sigma\Delta t}{2\varepsilon}}{1+\frac{\sigma\Delta t}{2\varepsilon}}E_x^q\left(m+\frac{1}{2},n,p\right)+\frac{1}{1+\frac{\sigma\Delta t}{2\varepsilon}}\left\{\frac{\Delta t}{\varepsilon\Delta y}\left[H_z^{q+\frac{1}{2}}\left(m+\frac{1}{2},n+\frac{1}{2},p\right)-H_z^{q+\frac{1}{2}}\left(m+\frac{1}{2},n-\frac{1}{2},p\right)\right]-\frac{\Delta t}{\varepsilon\Delta z}\left[H_y^{q+\frac{1}{2}}\left(m+\frac{1}{2},n,p+\frac{1}{2}\right)-H_y^{q+\frac{1}{2}}\left(m+\frac{1}{2},n,p-\frac{1}{2}\right)\right]\right\} \quad (12)$$

$$E_y^{q+1}\left(m,n+\frac{1}{2},p\right)=\frac{1-\frac{\sigma\Delta t}{2\varepsilon}}{1+\frac{\sigma\Delta t}{2\varepsilon}}E_y^q\left(m,n+\frac{1}{2},p\right)+\frac{1}{1+\frac{\sigma\Delta t}{2\varepsilon}}\left\{\frac{\Delta t}{\varepsilon\Delta z}\left[H_x^{q+\frac{1}{2}}\left(m,n+\frac{1}{2},p+\frac{1}{2}\right)-H_x^{q+\frac{1}{2}}\left(m,n+\frac{1}{2},p-\frac{1}{2}\right)\right]-\frac{\Delta t}{\varepsilon\Delta x}\left[H_z^{q+\frac{1}{2}}\left(m+\frac{1}{2},n+\frac{1}{2},p\right)-H_y^{q+\frac{1}{2}}\left(m-\frac{1}{2},n+\frac{1}{2},p\right)\right]\right\} \quad (13)$$

$$E_z^{q+1}\left(m,n,p+\frac{1}{2}\right)=\frac{1-\frac{\sigma\Delta t}{2\varepsilon}}{1+\frac{\sigma\Delta t}{2\varepsilon}}E_z^q\left(m,n,p+\frac{1}{2}\right)+\frac{1}{1+\frac{\sigma\Delta t}{2\varepsilon}}\left\{\frac{\Delta t}{\varepsilon\Delta x}\left[H_y^{q+\frac{1}{2}}\left(m+\frac{1}{2},n,p+\frac{1}{2}\right)-H_y^{q+\frac{1}{2}}\left(m-\frac{1}{2},n,p+\frac{1}{2}\right)\right]-\frac{\Delta t}{\varepsilon\Delta y}\left[H_x^{q+\frac{1}{2}}\left(m,n+\frac{1}{2},p+\frac{1}{2}\right)-H_x^{q+\frac{1}{2}}\left(m,n-\frac{1}{2},p+\frac{1}{2}\right)\right]\right\} \quad (14)$$

2.2. Stability criteria for FDTD

The stability of FDTD numerical solution was described by Taflove (1988) and was simplified by Sheen et al. (1990) by setting the spatial step size (δ) arbitrarily equal to one of the dimensions in the unit cell. In this study, Δx is chosen to be equal to δ, and the ratio of the other two dimensions with respect to Δx are; $r_y = \Delta y/\Delta x$; and $r_z = \Delta z/\Delta x$:

$$S=\frac{c\Delta t}{\delta}\leqslant\frac{1}{\sqrt{1+\frac{1}{r_y^2}+\frac{1}{r_z^2}}} \quad (15)$$

where S is the Courant number and c is the speed of light. The MATS-CSM was discretized such that the unit cell had a maximum size of 4 mm by 4 mm by 16 mm. These values gave an $r_y = 1$ and $r_z = 4.0$. The stability index of the entire computational volume would be 0.6963, which is greater than the Courant limit for a 3D model (i.e., $1/\sqrt{3} \approx 0.5574$) (Taflove, 2005); hence, Eq. (15) was satisfied. Furthermore, the mesh size for the dielectric media (i.e., food and water in the cavities) in the MATS-CSM was refined to have a smaller cell size complying with the 10 points per wavelength rule (Pathak et al., 2003).

2.3. Components of MATS-CSM

Since coupled microwave and heat transfer heating occurs only in the heating section of the MATS, other sections (i.e., preheating, holding and cooling sections) are not included in the MATS-CSM. Fig. 2 depicts the computational volume of the MATS-CSM. For simplicity, the waveguides that connect the cavities to their designated generators (e.g, cavity 1 waveguide connection to generator 1) are not included. Instead, they were replaced by two ports located at the top and bottom portion of the horn applicator (Fig. 2B(a)).

2.4. Food representation in MATS-CSM

Whey protein gel (WPG) containing 75.4% moisture, 0.6% salt, 1% D-ribose, 18% WPG-392, and 5% WPG-895I was used as the model food. The procedure described by Pandit et al. (2007a,b) in preparing WPG was implemented in this study. The dielectric and thermal property of WPG was used to define food as a lossy material in the MATS-CSM. The whey protein gel slab (Fig. 2B(c)) set to move along different sections of MATS was represented in the simulation model by drawing an object consisting of: (a) a slab element in the middle with dimensions of 52 × 95 × 16 mm (i.e., x,y,z); (b) four-4 half cylinder elements attached to the four sides of the slab element, each with a radius equal to 16 mm and a length equal to the length of the side of the slab to which the half cylinder was attached; and (c) four-4 quarter sphere elements attached to the four corners of the slab element with radii equal to 16 mm.

Typical food products in pouches previously processed in the MATS contain sauce. To consider the sauce in the MATS-CSM model, the dielectric and thermal properties of commercially available Bertolli™ Alfredo sauce (Englewood Cliffs, NJ 07632) was used. The object representing Alfredo sauce was incorporated in the model in the same manner as the WPG. The final dimensions of the Alfredo sauce were (95 × 140 × 16 mm) (i.e., x,y,z). The volume occupied by the object representing WPG (94 × 127 × 16 mm) was embedded in the object representing the Alfredo sauce, displacing an equal volume occupied by the Alfredo sauce.

2.5. Dielectric and thermal property of WPG and Alfredo sauce

Dielectric property (DP) of WPG and Bertolli™ Alfredo sauce was measured using Hewlett-Packard 8752C network analyzer (Palo Alto, CA 94304). The dielectric property system and methodology described by Wang et al. (2003) was used in this study. Thermal properties of WPG and Bertolli™ Alfredo sauce were measured using a Decagon™ KD2-pro (Pullman, WA 99163). The specific heat and thermal conductivity were measured using the double needle method (Campbell et al., 1991). For the measurement of specific heat and thermal conductivity, a solid WPG sample was placed inside the same test cell used for dielectric property measurement described in Wang et al. (2003). The test cell was connected to a circulating oil bath for control of the sample temperature. The double needle probe of the Decagon™ KD2-Pro consisted of a line heat source at a fixed distance parallel to a temperature sensor carefully inserted into the WPG sample inside the test cell. As prescribed by Decagon, in using KD2-Pro, the pump for the circulating oil bath was turned off just before taking a measurement, to ensure no

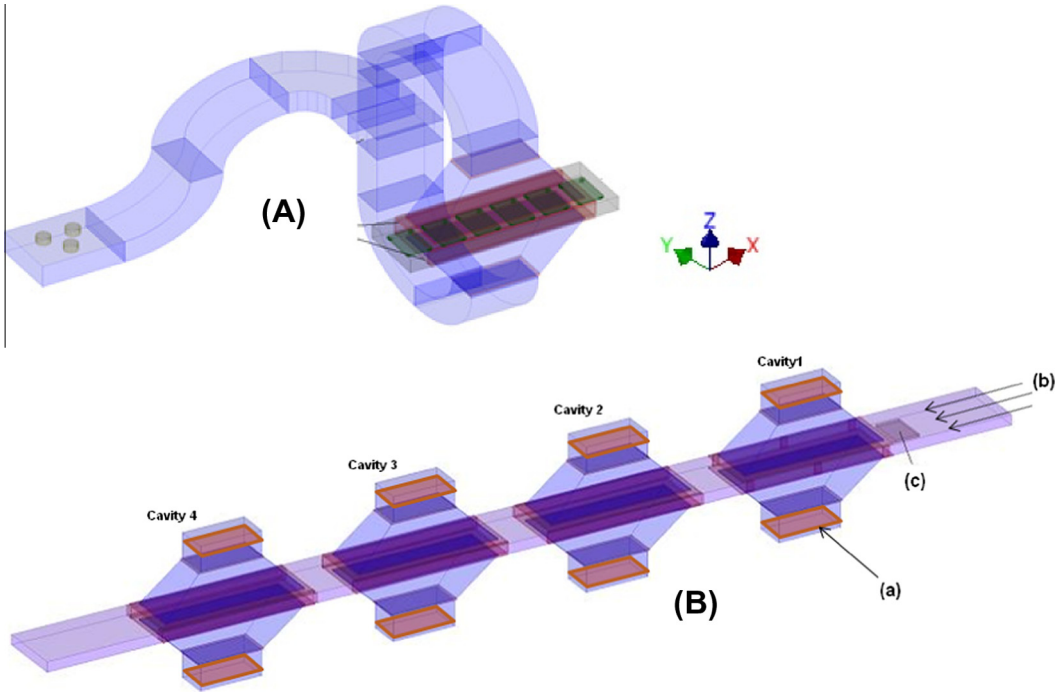

Fig. 2. (A) A representative cavity showing the waveguide configuration. (B) Simplified computational volume of MATS-CSM consisting of four microwave cavities and four pairs of horn applicators: (a) location of microwave input port (total of 8 ports); (b) direction of movement of pouch; (c) initial location of pouch.

Table 1
Different input ports in MATS-CSM.

Cavity	Ports	Frequency (MHz)	Net Transmitted Power (kW)	Amplitude (V/m)
Cavity 1	topPortCl bottomPortCl	912.1	6.40	80.0
Cavity 2	topPortC2 bottomPortC2	916.5	5.56	74.6
Cavity 3	topPortC3 bottomPortC3	905.6	2.51	50.1
Cavity 4	topPortC4 bottomPortC4	903.1	2.59	50.9

mechanical vibration interfered.The dielectric and thermal property measurement was made over a temperature range of 20–120 °C with 20 °C and 10 °C increment, respectively. Furthermore, using the measured data, dielectric and thermal properties of WPG and Alfredo sauce were extrapolated up to 150 °C and interpolated at 10 °C increment. Cubic spline or piecewise-polynomial approximation (Burden and Faires, 2005) was used to extrapolate and interpolate data points.

2.6. Input ports and designation of power level

Using FDTD to solve the electromagnetic equations on microwave heating requires definition of a microwave source, and dissipation of microwave power as heat in the load (i.e., the food). For the source of microwaves, typically, an input port is defined at a location within the computational volume. An input port covers an area in the computational volume, wherein the electric and magnetic field at a selected frequency is triggered at a known amplitude and excitation waveform (QWED, 2009). In the MATS-CSM there are eight input ports consisting of four top-ports and four bottom-ports (i.e. two ports for each cavity). Ports were drawn within the top and bottom standard WR975 waveguide attached to the tapered end of every horn (Fig. 2B(a)). The parameter settings of ports are summarized in Table 1.

The equivalent power injected at the input ports (Fig. 2B(a)) depends on the amplitude of the electric fields. Given the actual time-averaged power available from the microwave source (i.e., magnetron), the amplitude of the electric field at every input port should be equal to the square root of the time-maximum power (QWED, 2009):

$$A = \sqrt{2P} \tag{16}$$

where A is the amplitude of the electric field in the input port, P is the time-average power and $2P$ is the time-maximum power available from the source. Since there is a microwave reflection in the actual MATS system, the amplitude of the electric field at the ports in the simulation model was adjusted accordingly by considering only the net transmitted power. Using directional couplers manufactured by Ferrite Microwave, Inc. (Nashua, NH 03060), reflected power was measured for each cavity and only the corresponding transmitted powers (Table 1) were used in the MATS-CSM model. The equation for time-average power was given by Poynting's Theorem (Balanis, 1989):

$$P = \frac{1}{2}\Re(\vec{E} \times \vec{H}^*) \tag{17}$$

where P is the time-average power and the real part of the cross product of the electric field ($\vec{E}$) and the conjugate of magnetic field ($\vec{H}^*$) is the time-maximum power.

Dissipated power as heat ($\wp_v$) was derived from Eq. (17) by considering a closed surface of volume to which the power will be dissipated (e.g., the surface of the food):

$$\wp_v = 2\pi f \varepsilon_0 \varepsilon_r'' |E^2| \tag{18}$$

The frequency (f) of generators providing microwave energy was measured using a B&K Precision TM-6250 handheld spectrum analyzer with AN-301 antenna (Yorba Linda, CA 92887). The tabulated frequencies in Table 1 are the average frequency of each generator monitored for a period of one year (measured every other month).

Table 2
Simulation schedule to determine optimum $\Delta\tau$.

Step	Discretized movement step (mm)	Discretized heating time step ($\Delta\tau$) (s)	Estimated computational time* (h)
16	193.3	11.3	19
32	96.6	5.6	42
64	48.3	2.8	111

* Workstation specification: (1) Model number: HP-Z800, (2) processor: Intel Xeon X5680 @3.33 GHz, (3) memory: 96 GB DDR3 and (4) system type: 64-bit Windows 7 operating system.

2.7. Heat transfer boundary condition

In this study, a slab of whey protein gel (WPG) in Alfredo sauce packaged in a 160 × 110 × 16 mm flexible pouch was used as the food sample. It was assumed that the Alfredo sauce was viscous enough to cause insignificant movement during processing. Therefore, although WPG and Alfredo sauce each have unique dielectric and thermal properties as a function of temperature, both were considered as one solid food as far as heat transfer is concerned. Therefore, heat transfer within the food follows straightforward conduction model.

$$\nabla^2 T - \frac{c\rho}{k}\frac{\partial T}{\partial t} = 0 \tag{19}$$

However, at the boundary between the food and circulating water, heat flux (ψ) is governed by convective heat transfer:

$$\psi = -h(T - T_s) \tag{20}$$

where T is the temperature of the food at the boundary, T_s is the temperature of the circulating water, and h is the convective heat transfer coefficient. The convective heat transfer coefficient was approximated using the Dittus–Boelter correlation (Incropera et al., 2007)

2.8. Food movement and translation

The simulation routine was terminated after the completion of the discretized movement of food. The heating section of the MATS had a fixed length of 3.1 m and discretizing the movement of food means discretizing the total heating time as well. For example, if the desired microwave heating time in the MATS was set to 180 s, in simulation, and if the total length was discretized into 16 steps, each step would be 3100/16 = 193 mm and equivalent to 180/16 = 11.25 s of heating, which is the $\Delta\tau$.

In numerical simulation of time dependent processes, selection of appropriate heating time step, $\Delta\tau$, is very important since it determines convergence of thermal diffusion. A very large $\Delta\tau$ (i.e., few discretized steps) might cause immediate divergence. The simulated temperature within the food might be unrealistically low. To this end, it is important to determine the optimum $\Delta\tau$ that will allow solutions to converge at a reasonable simulation time. Table 2 summarizes the simulation schedule to determine an optimum $\Delta\tau$. For the three simulations conducted, all parameters except for the number of steps (heating time step, and movement step) were the same. The snapshots of heating patterns were taken at the center of the food with respect to its thickness in the z direction.

2.9. Simulation routine

The simulation routines of the MATS-CSM were adopted from the routine described by Celuch et al. (2011). Upon exporting the necessary files from the QuickWave™ Editor to the QuickWave™ Simulator, the EM field distribution within the computational volume was solved iteratively until steady state. After steady state was achieved, the average dissipated power was determined for every cell within the computational volume. The average dissipated power was calculated considering the effective conductivity of the lossy medium at an initial temperature (T_o). The volumetric enthalpy of each of cells was updated using:

$$Enthalpy^{j+1}(x,y,z) = Enthalpy^{j}(x,y,z) + \frac{\wp_v(x,y,z) * \Delta\tau}{\Delta V(x,y,z)} \tag{21}$$

where j and $\Delta\tau$ are the discretization of heating time and heating time step, respectively, and ΔV is the volume of the cell. The updated volumetric enthalpy [$Enthalpy^{j+1}(x,y,z)$], say for WPG and Alfredo sauce, corresponded to a higher temperature. The updated temperature was interpolated from the material property file of every lossy material (e.g., WPG and Alfredo Sauce):

$$T^{j+1}(x,y,z) = T[Enthalpy^{j+1}(x,y,z)] \tag{22}$$

2.10. Electromagnetic field distribution and symmetry

In the study by Chen et al. (2007, 2008), Ultem™ slab (Plastic International – Eden Prairie, MN 55344) was used to control electromagnetic field distribution inside the cavities of MATS. This was done by placing the Ultem™ slab of a certain thickness against the narrow walls of the cavities of MATS parallel to the direction of field propagation. Ultem™ has a relative dielectric constant and loss factor of 3.2 and 0.005, respectively, at 915 MHz. The prescribed placement and thickness of Ultem™ slab in Chen et al. (2008) was adapted in this study to come up with a staggered arrangement of the electric field pattern as food packages moved from one cavity of the MATS to the next.

Electromagnetic field distribution in cavities of MATS (i.e., with Ultem™ slab on the narrow walls of cavities) was determined using MATS-CSM on two simple scenarios: (1) the electromagnetic field distribution in empty cavities (i.e., cavities containing only water and no food); and (2) the electromagnetic field distribution for loaded cavities (i.e., cavities that contained both water and food). The snapshot of the electromagnetic field distribution for each cavity was taken after the MATS-CSM reached a steady state condition. For the first scenario, snapshots of the EM field distribution at the *xy*, *yz*, and *xz* planes were taken at a specified phase of the excitation voltage (all the snapshots were taken at the same phase). For the *xy* and *yz* plane snapshots, the centers of the computational volume along the *z* direction and the *x* direction were considered, respectively. For the *xz* plane, the center of each cavity along the *y* direction was considered. For the second scenario, a food was situated at the geometric center of each cavity. A snapshot of the EM field distribution was taken at a specified phase of the excitation voltage as with the first scenario along the *xy* plane at the center with respect to the *z* direction. Furthermore, the snapshot of the corresponding average dissipated power was taken. The color bar range used for all EM field distributions was from 0 to 200 V/m, while the color bar range for the dissipated power is from 0 to 10 MW/m^3.

2.11. Heating pattern in food estimated from coupled solution of EM-Heat transfer

This part of the study evaluated the importance of coupling heat transfer with the electromagnetic solution in terms of the resulting heating pattern in the WPG. Using the 32 step procedure (i.e., $\Delta\tau$ = 5.625 s and movement step = 96.6 mm) two simulations were performed: (a) electromagnetic-heat transfer coupled simulation, and (b) electromagnetic simulation without heat transfer.

(a) For the electromagnetic-heat transfer coupled simulation, the convective heat transfer coefficient (h) used was 115 W/m^2 K calculated using Dittus–Boelter correlation (Incropera et al., 2007).
(b) For the simulation without heat diffusion, only the dissipated power from the microwave energy was used as the source heat. Therefore, the boundary condition between the water-Alfredo sauce and the water-WPG was adiabatic.

2.12. Validation of the MATS-CSM using the chemical marker method

To validate computer simulation results, a chemical marker method on WPG was used (Pandit et al., 2007a,b). A 162 ± 5 g sample of WPG was cut into a slab with dimensions of 84 × 127 × 16 mm and packed into a 237 mL flexible pouch with 65 ± 1 g of Alfredo sauce. Six (6) sample pouches were loaded onto the microwave belt through the door and moved to the preheating section of the MATS. After 30 min of preheating at 70–72 °C, the generators powering the MATS, at the setting described in Table 1, were activated. The gauge pressure inside the MATS was maintained at 234.4 kPa. The temperature within the heating and holding sections was maintained at ~122 °C and the cooling section at ~20 °C. The belt holding the pouches of the WPG was moved at a speed of ~1.7 cm/s, allowing transition from preheating, heating, holding and finally to the cooling section. This translates into 3 min (180 s) of microwave heating. The WPG inside the pouch was allowed to cool in the cooling section for 5 min before retrieving it through the cooling section door.

The heating patterns of six processed samples of WPG 16 mm thick slabs were determined using the computer image analysis method as part of the chemical marker method described by Pandit et al. (2006, 2007a,b). In brief, each sample of processed WPG was cut in the middle layer along its thickness into two halves of 8 mm thickness with the aid of 8 mm spacer. Using a high definition camera (Nikon™ D70 with AF-S DX NIKKOR 18-55 mm f/3.5–5.6 G VR lens) (Nikon Inc. Melville, NY 11747) images from the cut layer in the center of the WPG (i.e, the xy plane) were taken and prepared for color analysis. Adobe Photoshop™ CS4 (Adobe Systems Incorporated, 345 Park Avenue San Jose, CA 95110) was used to prepare the images, and IMAQ Vision, a part of the library of LabVIEW (National Instrument product, Austin, TX 78759) was used to determine the RBG equivalent of browning in WPG. Browning in the WPG was produced as a result of the non-enzymatic reaction between sugar (D-ribose) and protein (WPG 392 and WPG 895-I) (Lau et al., 2003; Pandit et al., 2006).

Validation of the heating pattern was conducted by comparing the prominent temperature zones in a given area in the heating pattern of the chemical marker method, and mapping it with the result generated by the MATS-CSM. The location of the temperature zones and the weighted average of temperature from the areal cross section in a given zone was the basis for validation.

3. Results and discussion

3.1. Dielectric and thermal property of materials

The dielectric properties at 915 MHz and thermal properties of the whey protein gel (WPG) and the Alfredo sauce are summarized in Tables 3 and 4 respectively. Values corresponding to 20 °C, 40 °C, 60 °C, 80 °C, 100 °C, and 120 °C were measured. Other values were

Table 3
Dielectric properties at 915 MHz and thermal properties of whey protein gel (WPG).

Temperature (°C)	Dielectric constant ε' (unit less)	Loss factor ε'' (unit less)	Effective conductivity $2\pi f\varepsilon_0\varepsilon''$ (S/m)	Specific heat (kJ/kg °C)	Thermal conductivity (W/m °C)	Enthalpy (MJ/m^3)
20	52.91 ± 2.49	23.58 ± 2.75	1.20	2.94[b]	0.40[b]	–
40	51.76 ± 0.99	29.26 ± 1.01	1.49	3.08[b]	0.45[b]	–
60	50.62 ± 0.77	34.85 ± 1.53	1.77	3.21 ± 0.11	0.50 ± 0.02	–
70	50.03[a]	39.75[a]	2.02	3.28 ± 0.18	0.52 ± 0.04	0
80	49.35 ± 1.45	41.68 ± 1.97	2.12	3.35 ± 0.04	0.54 ± 0.01	26.77
90	48.89[a]	46.76[a]	2.38	3.41 ± 0.03	0.56 ± 0.01	60.91
100	48.11 ± 1.74	50.73 ± 1.74	2.58	3.48 ± 0.06	0.57 ± 0.01	95.72
110	47.76[a]	53.77[a]	2.74	3.55 ± 0.02	0.59 ± 0.01	131.21
120	47.42 ± 1.15	58.40 ± 3.02	2.97	3.62 ± 0.10	0.60 ± 0.01	167.37
130	46.63[b]	60.78[b]	3.09	3.68[b]	0.61[b]	204.20
140	46.06[b]	64.28[b]	3.27	3.75[b]	0.62[b]	241.70
150	45.49[b]	67.79[b]	3.45	3.82[b]	0.63[b]	279.87

[a] Interpolated values.
[b] Extrapolated values.

Table 4
Dielectric properties at 915 MHz and thermal properties of Alfredo sauce.

Temperature (°C)	Dielectric constant ε' (unit less)	Loss factor ε'' (unit less)	Effective conductivity $2\pi f\varepsilon_0\varepsilon''$ (S/m)	Specific heat (kJ/kg °C)	Thermal conductivity (W/m °C)	Enthalpy (MJ/m^3)
20	55.11 ± 0.45	43.09 ± 3.08	2.19	3.73	0.514	–
40	52.60 ± 0.32	57.44 ± 1.29	2.92	3.62	0.522	–
60	49.67 ± 0.52	73.52 ± 1.96	3.74	3.64	0.546	–
70[a]	48.56[a]	81.20[a]	4.13	3.59	0.555	0.00
80	47.06 ± 0.69	88.88 ± 2.94	4.52	3.52	0.550	35.22
90[a]	45.91[a]	97.03[a]	4.94	3.55	0.552	70.69
100	44.14 ± 1.36	105.68 ± 3.29	5.38	3.54	0.552	106.08
110[a]	43.26[a]	113.15[a]	5.76	3.61	0.558	142.14
120	41.47 ± 1.91	120.98 ± 2.86	6.16	3.73	0.572	179.43
130[b]	40.61[b]	129.53[b]	6.59	3.92	0.597	218.60
140[b]	39.28[b]	137.83[b]	7.02	4.16	0.629	260.16
150[b]	37.96[b]	146.19[b]	7.44	4.45	0.671	304.68

[a] Interpolated values.
[b] Extrapolated values.

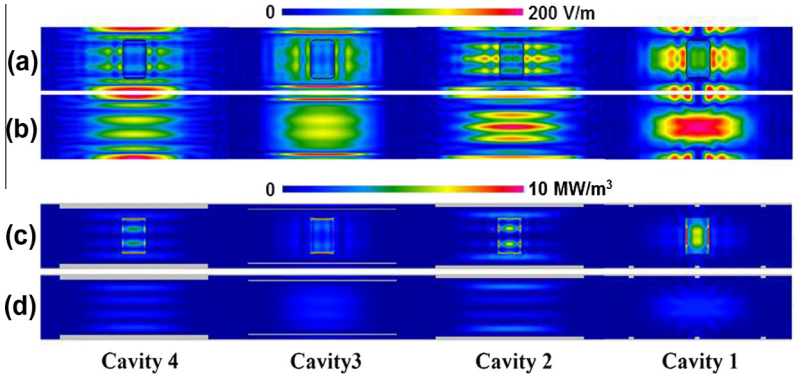

Fig. 3. Electric field distribution (range from 0 to 200 V/m) in the *xy* plane at the center of the cavity for: (a) loaded cavities, and (b) unloaded cavities. Dissipated power density (range from 0 to 10 MW/m^3) in the *xy* plane at the center of the cavity for: (c) loaded cavities, and (d) unloaded cavities.

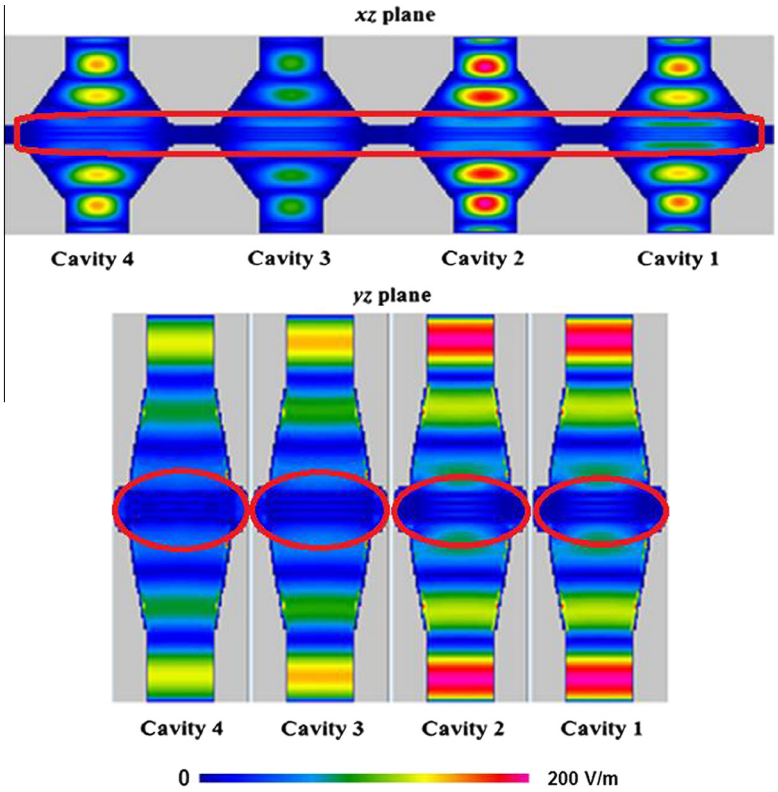

Fig. 4. Electric field distribution in the *xz*, and *yz* plane. The *xz* plane was taken at the center with respect to *y* axis. The *yz* plane was taken at the geometric center of each cavity *x* axis.

either interpolated or extrapolated from the measured properties. These data were used to define the food as lossy materials (WPG and Alfredo sauce) in the MATS-CSM.

3.2. Electromagnetic field distribution and symmetry

Fig. 3 shows the electric field distribution (V/m) at steady state along the *xy* plane at the center of the cavity traversing the center of the food with respect to the *z* axis. Fig. 3a includes water and food pouches located at the center of each cavity. Fig. 3b shows the electric field distribution in circulating water without food. From Fig. 3b, a consistent electric field distribution was observed at a given phase within the cavities considering the frequencies and power settings of generators described in Table 1. Thus, in every cavity the electric field distribution is predictable and symmetrical along the *xy* plane. With the presence of food (Fig. 3a), the electric field distribution was still predictable and exhibited a similar pattern at a given phase as shown in Fig. 3b.

The placing of the Ultem™ bars on the walls of each cavity was successful in creating a staggered electric field distribution for every cavity (Chen et al., 2008). For example, in cavity 1, the *E* field was concentrated at the center, then in cavity 2, the *E* field was concentrated along the sides of the food as shown by three strips of *E* field pattern, then in the center again for cavity 3, and finally at the side again for cavity 4 (Fig. 3b). The effect of the staggered electric field distribution produced a relatively uniform heating pattern in the food as it traversed the four cavities.

The staggered arrangement of the electric field is more visible in the dissipated power distribution (Fig. 3c and d). In this illustration, in cavity 1, the power was mostly dissipated toward the

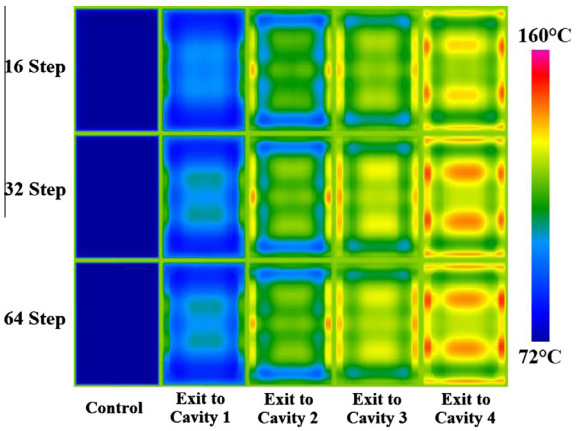

Fig. 5. MATS-CSM result for temperature distribution in WPG using different heating time step (16 step, 32 step, and 64 step). The first column represent the initial temperature of the food (control), and the second, third, fourth and fifth column show the heating pattern of the food at the exit of first, second, third, and fourth, cavity respectively.

middle of the food. For cavity 2, the power was dissipated horizontally along the side of the food, for cavity 3 toward the middle of the food, and finally for cavity 4 toward the side again.

The *xz* and *yz* plane views of the electromagnetic field distribution (Fig. 4) show the symmetry of the electric field in the *z* direction. Since the pattern is symmetrical, the two electric fields from the top and bottom port of each cavity are in-phase. Fig. 4 also illustrates the standing wave patterns inside the cavities (i.e., area under the red markings). The three distinct horizontal lines at the center of each cavity are the standing wave pattern resulting from the interaction of the incident field from the top and bottom horn. Notice that the middle horizontal line is exactly at the center of the cavity with respect to the *z* direction indicating a high intensity of electric field at the location of the food.

3.3. Food movement and translation

In Fig. 5, starting at the control, it can be noticed that the temperature distribution was uniform at 72 °C and as the food moved through different cavities, the heating pattern changed. There were no differences however in the heating patterns among 16, 32, and 64 heating time steps for a food within a given cavity. The total heating time used was 180 s and the heating time for each step is 11.25 s, 5.63 s, and 2.81 s for 16, 32, and 64 heating time steps.

Although the heating patterns were the same for 16 and 32 heating time steps, the temperature distribution ranges were noticeably different. Considering the 16 and 32 heating time steps at the exit to cavity 4 (Fig. 5), the temperature predicted using step 16 is much lower (e.g., 130 °C in the hot area) than step 32 (e.g., 135 °C for the hot area). There were no significant differences in the temperature distribution for steps 32 or 64. These findings suggest that simulating with less than 32 steps is not recommended because of the likelihood of immediate divergence of solution. Specifically, the heating time step ($\Delta\tau$) used in the 16 step simulation is too large ($\Delta\tau$ = 11.3 s), as indicated by a higher range temperature distribution. On the other hand, simulating with more than 32 steps is not practical because a similar solution will be obtained despite the longer simulation time. Therefore, in this study the optimum time step was 5.6 s (each movement step being 97 mm), which corresponds to 32 steps or 32-discretization in the heating time and displacement for the complete translation of the food pouch through the four cavities. The approximate simulation time for 32 steps was 42 h per simulation run.

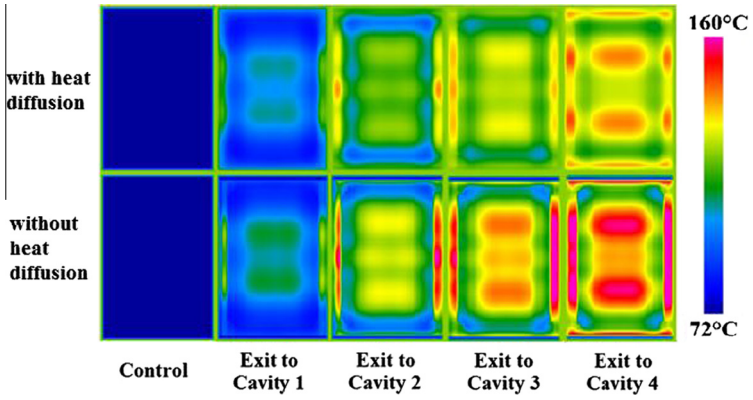

Fig. 6. Comparison of heating pattern for electromagnetic coupled heat transfer simulation (with heat diffusion) and electromagnetic simulation alone (without heat diffusion). Both simulations were executed on a 32-step simulation.

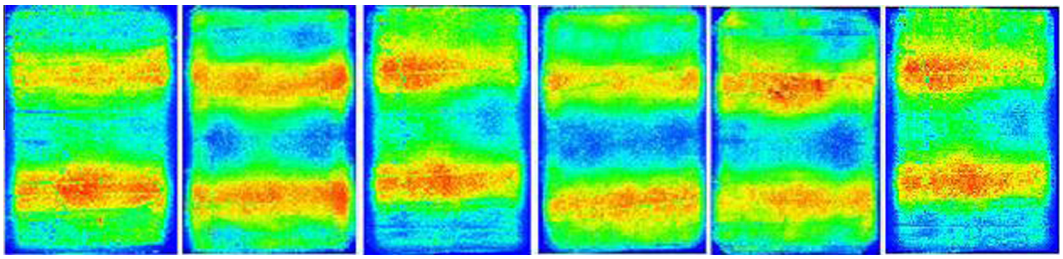

Fig. 7. Six (6) replicates of heating pattern in whey protein gel (WPG) determined through chemical marker method. Images were a snapshot of *xy* plane of WPG at the center with respect to *z*-axis.

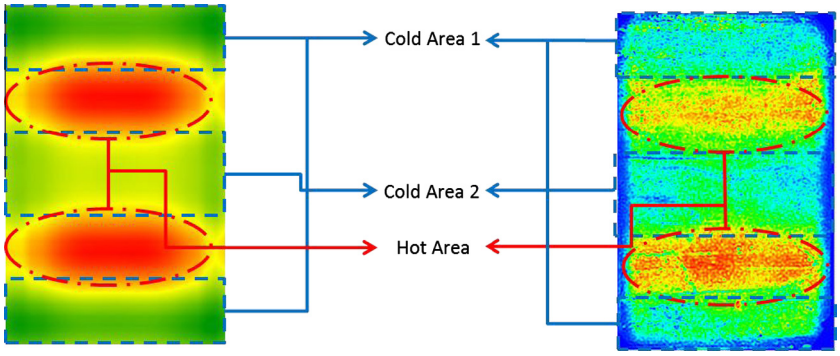

Fig. 8. Comparison of heating pattern generated from (a) MATS-CSM model and (b) chemical marker method on WPG.

Since using 32 steps, with a heating time step of 5.6 s and movement step of 97 mm, was identified as the optimum condition, successive simulations were based on 32 steps.

3.4. Comparison of the microwave heating patterns of the simulation model with and without the surface heat transfer function

This section compares the results of heating patterns generated by computer simulation for two scenarios: (1) microwave heating without heat diffusion, and (2) combined microwave heating with heat diffusion through heat conduction within the food and heat convection on the surface of the food. One of the obvious effects of not incorporating heat diffusion in the solution of the electromagnetic field would be a more uneven distribution of temperature. Removing the heat transfer function from the MATS-CSM resulted in accumulation of dissipated power in the cell throughout the microwave heating time due to the adiabatic boundary condition. Cells exposed to higher electric fields dissipated more power (resulting in a higher temperature) than cells exposed to lesser electric field. In Fig. 6 without heat diffusion, the lowest temperature at the corner of the food at the exit to cavity 4 was about 72–75 °C, while the highest temperature was already at 150–155 °C. Considering actual processing in MATS, the large difference in temperature at the corner of the food is not possible because of the circulating water. Circulating water causes thermal diffusion at the surface of the food such that the flux may act as either a heat sink or a heat source which evens out temperature distribution at the surface.

For simulation that allows heat diffusion (Fig. 6 with heat diffusion), the difference between maximum and minimum temperature at the exit to cavity 4 was relatively smaller (~18 °C) as compared to that of Fig. 6 without heat diffusion (~50 °C). Furthermore, allowing heat diffusion within the food and at the interface of food and circulating water (using 115 W/m^2 K as the heat transfer coefficient) results in an overall decrease in the temperature of the hot spots in the food (Fig. 6 with heat diffusion) making the temperature distribution relatively uniform (lowest and highest temperature range was approximately at 110–113 °C and 132–135 °C, respectively). Fig. 6 with heat diffusion illustrates the advantage of having circulating water inside the cavities. Circulating water reduces the edge heating effect in the food, and reduced the range of the temperature distribution in the food resulting in a relatively uniform heating pattern.

3.5. Validation of computer simulation model using a chemical marker method

Fig. 7 shows the result of six replicates of the heating patterns in the WPG as indicated by the accumulated chemical marker (M-2) (Pandit et al., 2007a,b). The results of the chemical marker method, unlike those of the simulation result, were not perfectly symmetrical with respect to the *xy* plane. The unsymmetrical heating pattern in the WPG could be due to: (a) relative position of WPG during processing in the MATS, (b) procedural errors in cutting of the whey protein gel along its thickness, (c) pockets of air inside the pouch, (d) micro-bubbles within the WPG, and (e) possible moisture migration during processing of the WPG.

Fig. 8 compares the heating patterns between the results of the MATS-CSM and the chemical marker method on the WPG. Fig. 8a shows a snapshot of the heating pattern taken from the 32-step simulation at the end of the fourth cavity with the heat transfer function using 115 W/m^2 K as the heat transfer coefficient (h). Fig. 8b is a representative heating pattern result of the chemical marker method.

The heating pattern of the MATS-CSM model and the chemical marker on the WPG can be summarized into three general temperature zones:

- *Cold Area* 1. These were the upper- and lower-most areas within the *xy* plane. Since the heating pattern and temperature distribution is symmetrical in the *xy* plane, these areas were designated as one (i.e., Cold Area 1).
- *Cold Area* 2. This area was at the middle of the *xy* plane.
- *Hot Area*. These areas were the two intensely colored areas between cold area 1 and cold area 2. Since the two hot areas are symmetrical they were designated as one (i.e., Hot Area).

Based on the result of the MATS-CSM simulation, the combined area of cold area 1 and hot area comprises approximately 35% and 40% of the total area in the *xy* plane, respectively, while cold area 2 comprises approximately 25%. The simulated average temperatures in the cold area 1, hot area, and cold area 2 were 112 °C, 134 °C, and 121 °C, respectively. Therefore, the areal weighted average temperature of the result of the MATS-CSM (Fig. 8a) was 123 °C. From the results of the chemical marker method on the WPG (Fig. 8b), the approximate areal percentage for cold area 1, cold areas 2, and hot area, were 35%, 30%, and 35%, respectively. However the color value indicated by the chemical marker method cannot be directly correlated to temperature because the amount of M-2 marker formation depends on the accumulated thermal lethality for *C. botulinum* spores (F_o) and not on the final temperature (Pandit et al., 2007a,b). Therefore, Fig. 8b was more of a lethality pattern rather than a heating pattern. Nevertheless, for qualitative purposes, areas with high color value (reddish) received more lethality than areas with low color value (bluish). Since lethality is related to the time-temperature exposure of a certain area, the final temperature distribution pattern in Fig. 8a was comparable to the lethality pattern described by lethal rate (F_o) in Fig. 8b. Since the location, percent area, and the relative position of cold area 1, cold area 2, and hot area in Fig. 8a was similar to that

of Fig. 8b, the result of the MATS-CSM was verified to give accurate heating pattern, and therefore can be used as a tool for locating the cold spot in food.

4. Conclusion

The MATS-CSM was created to provide tools for better understanding of the theoretical concept of electromagnetic and heat transfer phenomena applied to microwave assisted sterilization of food. This computer simulation model was specific to modeling the heating section of the microwave assisted thermal sterilization (MATS) located at WSU. With the main objective of improving and addressing the limitations of the previous computer simulation model created by Chen et al. (2008) and in reference to the specific objectives, this study was able to accomplish the following:

- The standing wave created due to the interaction of the field was precisely at the center of the cavity with respect to the z direction indicating a high intensity of electric field at the location of the food.
- The optimum time step for the MATS-CSM was demonstrated to be 5.6 s, which corresponds to 32 steps or 32 discretization in heating time and movement of the food pouch across the four cavities of the heating section.
- Incorporating the heat transfer function into the electromagnetic solution in determining the heating pattern resulted in a relatively uniform and more accurate temperature distribution as compared to the solution without the heat transfer function. Furthermore, this study proves that circulating water in the cavity can alleviate the edge overheating effect.
- Based upon the percentage of area and the relative positions of cold area 1, cold area 2, and the hot area, the MATS-CSM gave accurate heating patterns, and therefore can be used as a tool for locating the cold spot in food.

References

Balanis, C.A., 1989. Advanced Engineering Electromagnetics. John Wiley & Sons Inc., New Jersey.

Brody, A.L., 2011. Advances in microwave pasteurization and sterilization. Food Technology 65 (2), 1–3.

Burden, R.L., Faires, J.D., 2005. Numerical Analysis, eighth ed. Thompson Brooks/Cole, Belmont, CA, USA.

Campbell, G.S., Calissendorff, C., Williams, J.H., 1991. Probe for measuring soil specific-heat using a heat-pulse method. Soil Science Society of America Journal 55 (1), 291–293.

Celuch, M., Kopyt, P., 2009. Modeling microwave heating in foods. In: Lorence, M.W., Pesheck, P.S. (Eds.), Development of Packaging and Products for Use in Microwave Ovens. Woodhead Publishing Limited and CRC Press LLC, Boca Raton, pp. 305–346.

Celuch, M., Soltysiak, M., Erle, U., 2011. Computer simulation of microwave heating with coupled electromagnetic, thermal, and kinetic phenomena. Applied Computational Electromagnetics Society Journal 26 (4), 275–284.

Chen, H., Tang, J., Liu, F., 2007. Couples simulation of an electromagnetic heating process using the finite difference time domain method. Journal of Microwave Power and Electromagnetic Energy 41 (3), 50–68.

Chen, H., Tang, J., Liu, F., 2008. Simulation model for moving food packages in microwave heating processes using conformal FDTD method. Journal of Food Engineering 88 (3), 294–305.

Decareau, R.V., 1985. Microwaves in the Food Processing Industry. Academic Press, Inc., Orlando, FL, USA.

Geedipalli, S.S., Rakesh, V., Datta, A.K., 2007. Modeling and heating uniformity contributed by rotating turntable in microwave oven. Journal of Food Engineering 82, 359–368.

Guan, D., Plotka, V.C.F., Clark, S, Tang, J, 2002. Sensory evalution of microwave treated macaroni and cheese. Journal of Food Processing and Preservation 26, 307–322.

Guru, B., Hiziroglu, H., 2004. Electromagnetic: Feild Theory Fundamentals, second ed. Cambridge University Press, New York.

Hossan, M.R., Byun, D., Dutta, P., 2010. Analysis of microwave heating for cylindrical shaped objects. International Journal of Heat and Mass Transfer 53 (23–24), 5129–5138.

Incropera, F.P., DeWitt, D.P., Bergman, T.L., Lavine, A.S., 2007. Introduction to Heat Transfer. John Wiley & Sons, Inc., Hoboken.

Kashyap, S.C., Wyslouzil, W., 1977. Method for improving heating uniformity of microwave ovens. Journal of Microwave Power and Electromagnetic Energy 12 (3), 223–230.

Kopyt, P., Celuch, M., 2003. Coupled electromagnetic and thermal simulation of microwave heating process. In: Barcelona: 2nd Internaltional Workshop on Information Technologies and Computing Techniques for the Agro-Food Sector, pp. 51–54.

Kopyt, P., Celuch, M., 2004. Coupled FDTD-FEM approach to modelling of microwave heating process. In: 5th IEE International Conference on Computation in Electromagnetics CEM. Stratford-upon-Avon, UK, pp. 171–172.

Lau, H., Tang, J., Taub, I.A., Yang, T.C., Edwards, C.G., Mao, R., 2003. Kinetics of chemical marker formation in whey protein gels for studying high temperature short rime microwave sterilization. Journal of Food Engineering 60, 397–405.

Metaxas, A.C., Meredith, R.J., 1993. Industrial Microwave Heating. Peter Peregrinus Ltd., London.

Pandit, R.B., Tang, J., Mikhaylenko, G., Liu, F., 2006. Kinetics of chemical marker M-2 formation in mashed potato – a tool to locate cold spots under microwave sterilization. Journal of Food Engineering 76 (3), 353–361.

Pandit, R.B., Tang, J., Liu, F., Mikhaylenko, G., 2007a. A computer vision method to locate cold spots in foods in microwave sterilization processes. Pattern Recognition 40 (12), 3667–3676.

Pandit, R.B., Tang, J., Liu, F., Pitts, M., 2007b. Development of a novel approach to determine heating pattern using computer vision and chemical marker (M-2) yield. Journal of Food Engineering 78, 522–528.

Pathak, S.K., Liu, F., Tang, J., 2003. Finite difference time domain (FDTD) characterization of a single mode applicator. Journal of Microwave Power and Electromagnetic Energy 38 (1), 1–12.

Pozar, D.M., 2005. Microwave Engineering, third ed. John Wiley & Sons, MA.

QWED, 2009. Basic heating module for QuickWave-3D electromagnetic simulator. In: QWED, Quickwave Software for Electromagnetic Design, 7.5 ed., QWED, Warsaw, pp. 1–78.

Risman, P., 2009. Advanced topics in microwave heating uniformity. In: Lorence, M.W., Pesheck, P.S. (Eds.), Development of Packaging and Product for Use in Microwave Ovens. CRC Press LLC, Boca Raton, FL, USA, pp. 66–104.

Romano, V.R., Marra, F., Tammaro, U., 2005. Modelling of microwave heating of foodstuff: study on the influence of sample dimensions with a FEM approach. Journal of Food Engineering 71 (3), 233–241.

Ryynanen, S., Ohlsson, T., 1996. Microwave heating uniformity of ready meals as affected by placement, composition, and geometry. Journal of Food Science 61 (3), 620–624.

Sheen, D.M., Ali, S.M., Abouzahra, M.D., Kong, J.A., 1990. Application of the three dimensional finite-difference time-domain method to the analysis of planar microstrip circuits. IEEE Transactions on Microwave Theory and Techniques 38 (7), 849–857.

Sundberg, M., Risman, P.O., Kildal, P.S., Ohlson, T., 1996. Analysis and design of industrial microwave ovens using the finite difference time domain method. Journal of Microwave Power and Electromagnetic Energy 31 (3), 142–157.

Taflove, A., 1988. Review of the formulation and applications of the finite-difference time-domain method for numerical modeling of electromagnetic wave interaction with arbitrary structures. Wave Motion 10 (6), 547–582.

Taflove, A., Hagness, S.C., 2005. Computational Electrodynamics: The Finite-Difference Time-Domain Method, third ed. Artech House, Norwood, MA.

Tang, J., Feng, H., Lau, M., 2002. Microwave heating in food processing. In: Young, X., Tang, J., Zhang, C., Xin, W. (Eds.), Advances in Agricultural Engineering. Scientific Press, New York.

Tang, J., Liu, F., Pathak, S.K., Eves, E.E., 2006. Patent No. US 7119313. USA.

Tang, Z., Mikhaylenko, G., Liu, F., Mab, J.H., Tang, J., Pandit, R., Younce, F., 2008. Microwave sterilization of sliced beef in gravy 7-oz trays. Journal of Food Engineering 89 (4), 375–383.

Wang, Y.F., Wig, T.D., Tang, J.M., Hallberg, L.M., 2003. Dielectric properties of food related to RF and microwave pasteurization and sterilization. Journal of Food Engineering 57, 257–268.